Available online at www.sciencedirect.com
SCIENCE DIRECT®
Journal of Sound and Vibration 292 (2006) 911–934
JOURNAL OF SOUND AND VIBRATION
www.elsevier.com/locate/jsvi

Acoustic scattering by a spliced turbofan inlet duct liner at supersonic fan speeds

A. McAlpine*, M.C.M. Wright

Institute of Sound and Vibration Research, University of Southampton, Southampton SO17 1BJ, UK

Received 18 October 2004; received in revised form 16 August 2005; accepted 15 September 2005
Available online 9 November 2005

Abstract

Fan noise is one of the principal noise sources generated by a turbofan aero-engine. At supersonic fan speeds, fan tones are generated by the "rotor-alone" pressure field. In general, these tones can be well absorbed by an inlet duct acoustic liner, apart from at high supersonic fan speeds. However, in practice inlet duct liners contain acoustically hard longitudinal splices which cause scattering. This leads to acoustic energy being scattered into a range of different azimuthal mode orders, similar to the modal content resulting from rotor–stator interactions. The effectiveness of an inlet duct lining is reduced because acoustic energy is scattered into modes that are poorly absorbed by the liner. In this article, the effect of this acoustic scattering is examined by three-dimensional finite-element simulations of sound transmission in a turbofan inlet duct. Results include predictions of the sound power transmission loss with different splice widths, and at different supersonic fan speeds. These results demonstrate how acoustic scattering by liner splices can adversely affect fan tone noise levels at low supersonic fan speeds, but have little adverse affect on noise levels at high supersonic fan speeds. The potential noise benefit that could be achieved by manufacturing thinner splices is also examined.

1. Introduction

There has been considerable success over the past 50 years in reducing commercial aircraft engine noise levels. Noise levels from modern turbofan aero-engines are lower than earlier generations of engine, owing largely to the development of high-bypass-ratio turbofan engines that has led to significant reductions in jet noise. However, the use of larger fans and inlet ducts means that fan noise generated by high-bypass-ratio turbofan aero-engines is nowadays one of the principal engine noise sources.

There are several well-known fan tone noise sources, including "rotor-alone" tones and "rotor–stator" interaction tones. Tyler and Sofrin [1] describe in detail the source generation mechanisms. Rotor-alone tones are due to the steady (in a frame of reference rotating with the fan), pressure field attached to a ducted fan. The tones have frequencies that are multiples of the engine's shaft rotation frequency, $\mathscr{F}$. At subsonic fan operating speeds, $M_t < 1$, the rotor-alone pressure field is cut-off; thus, rotor-alone tones are only an important noise source at supersonic fan speeds. In modern turbofan engines, the fan speed is supersonic at

*Corresponding author. Tel.: +44 23 8059 2291; fax: +44 23 8059 3190.
E-mail address: am@isvr.soton.ac.uk (A. McAlpine).

0022-460X/$ - see front matter © 2005 Elsevier Ltd. All rights reserved.
doi:10.1016/j.jsv.2005.09.010

Nomenclature

A	modal amplitude (Pa)
b	duct radius (m)
B	number of fan blades
BPF	blade passing frequency (Hz)
c	speed of sound ($\mathrm{m\,s^{-1}}$)
[**C**]	damping matrix
d	distance between fan plane and liner (m)
EO	engine order
f	frequency (Hz)
$\mathscr{F}$	engine shaft rotation frequency (Hz)
I_x	axial intensity ($\mathrm{W\,m^{-2}}$)
Im{}	denotes imaginary part
J_m	Bessel function of the first kind, order m
k	acoustic wavenumber ($\mathrm{rad\,m^{-1}}$)
kb	Helmholtz number (non-dimensional frequency)
k_x	axial wavenumber ($\mathrm{rad\,m^{-1}}$)
[**K**]	stiffness matrix
l	liner length (m)
L	duct length (m)
(m,n)	(azimuthal, radial) mode order
m_c	highest cut-on azimuthal mode order (ω fixed)
[**M**]	mass matrix
M_t	fan tip Mach number
M_x	axial Mach number
$\hat{\mathbf{n}}$	unit normal (outward)
n_c	highest cut-on radial mode order (m and ω fixed)
N_s	number of splices
p	pressure (Pa)
PWL	sound power level (dB)
r	radial coordinate (m)
rpm	revolutions per minute
R	resistance (non-dimensional)
Re{}	denotes real part
s	splice width (m)
SPL	sound pressure level (dB)
t	time (s)
u	velocity ($\mathrm{m\,s^{-1}}$)
U	axial mean flow ($\mathrm{m\,s^{-1}}$)
V	number of stator vanes
W	sound power (W)
x	axial distance upstream of the fan (m)
$\hat{\mathbf{x}}$	unit normal (x-direction)
X	reactance (non-dimensional)
Z	specific acoustic impedance (non-dimensional)

Greek letters

α_x	axial wavenumber, lined duct section ($\mathrm{rad\,m^{-1}}$)
γ	adiabatic constant
Γ	surface of the acoustic domain
Δ_{LAM}	least attenuated mode transmission loss (dB)
Δ_{PWL}	sound power transmission loss (dB)
ζ	cut-off ratio
θ	azimuthal coordinate (rad)
κ	radial wavenumber ($\mathrm{rad\,m^{-1}}$)
λ	acoustic wavelength (m)
μ	radial wavenumber, lined duct section ($\mathrm{rad\,m^{-1}}$)
ρ	density ($\mathrm{kg\,m^{-3}}$)
ϕ	velocity potential ($\mathrm{m^2\,s^{-1}}$)
ψ	mode shape function
ω	angular frequency $2\pi f$ ($\mathrm{rad\,s^{-1}}$)
Ω	acoustic domain

Subscripts

m,n	denotes mode (m,n)
0	denotes mean value

Superscripts

$'$	denotes an acoustic quantity
$\hat{}$	denotes a harmonic quantity
$+$	denotes a right-running mode
$-$	denotes a left-running mode
$\bigstar$	denotes value of a parameter at model scale

high-power operating conditions, such as during take-off and climb. Rotor-alone tones are the principal component of the so-called "buzz-saw" noise that is audible at high-power operating conditions.

Rotor–stator interaction tones are generated when the rotor blade wakes impinge on fixed stator vanes, or vice versa. The tones have frequencies that are multiples of blade passing frequency (BPF). At subsonic fan speeds, not all the components of the rotor–stator interaction pressure field will be cut-off. In modern turbofan engines, the fan speed is subsonic at low-power operating conditions, such as during approach. At

this low-power operating condition, the principal component of fan tonal noise is rotor–stator interaction tones.

Typically, in modern turbofan engines the inlet duct contains acoustic lining, which absorbs sound generated by the fan. This liner is usually manufactured in sections which each cover part of the duct's circumference. This facilitates the manufacture and installation of the lining inside the nacelle. The sections are joined together by longitudinal strips or splices. The splices will be acoustically hard. This means that there will be discontinuities in the acoustic impedance around the circumference of the duct.

In this article the effect, at supersonic fan speeds, of acoustic scattering caused by liner splices is examined. The area covered by the splices will be small, typically less than 5% of the total area of duct wall covered by the liner. Although this reduction in lined area is small, the splices cause additional azimuthal mode scattering. (Note that in general any non-uniformity in the inlet duct can cause scattering, for example distortion in the mean-flow, or the presence of inlet probes.) It will be shown that liner splices can significantly reduce the attenuation at supersonic fan speeds. This is because acoustic energy is scattered out of the rotor-alone field, and energy in the scattered field is less well absorbed by the acoustic liner.

The concept of non-uniform liners has been studied by several authors. For example, Lansing and Zorumski [2] in 1973 and Unruh [3] in 1976 examined the transmission of sound in an axially segmented lined duct, using mode-matching techniques. This type of axially segmented liner is of interest because it could be used to increase the attenuation of fan tones at high supersonic fan speeds; this will be examined in a subsequent article.

In a circular-section lined duct, with a circumferentially varying wall impedance, it is not possible to separate r and θ, in order to find analytic expressions for the modes of the duct. Watson [4] in 1981, and also Fuller [5,6] in 1984, proposed an analytic solution to this type of problem. The wave equation was solved by separating the x-dependence, and then expressing both the mode shapes $\psi(r,\theta)$ and wall impedance $Z(\theta)$ as Fourier series expansions in θ. Then, solutions can be found, in principle, by solving a system of eigenequations.

In 2001 Elnady et al. [7], using a similar approach to Watson and Fuller, formulated a numerical scheme for an arbitrary duct cross-section, with a circular central duct surrounded by a bulk absorber. The point-matching method was used to ensure the solutions satisfied the boundary conditions at a specified number of collocation points. More recently, they have applied this method to investigate the effect of hard strips in (locally reacting) lined ducts for application to aircraft engines [8]. More recently, Wright [9] matched analytic rigid-wall modes to modes in spliced liners that were obtained from a general purpose finite element (FE) Helmholtz solver for the no-flow problem.

The first numerical calculations of sound transmission in a duct with a circumferentially varying liner appear to have been by Watson [10] in 1977 and Astley et al. [11] in 1980. The results in Refs. [10] and [11] were obtained by using the FE method. Watson carried out calculations for a three-dimensional rectangular duct with no flow. Astley et al. formulated the problem for a uniform flow duct with arbitrary cross-section, and a circumferentially varying lining. At that time, these types of calculations were restricted to low frequencies, because the problem is not axisymmetric. For example, in Ref. [11] a circular duct calculation was conducted at Helmholtz number, or reduced frequency, $kb = 1$.

Examples of measurements of scattering by liner splices can be found in Rademaker et al. [12]. They measured the scattered sound field in a model turbofan inlet duct, using a mode detection array located near the exit plane. The inlet contained a locally reacting lining with 8 splices. The measurements in Ref. [12] clearly show that at some fan speeds the sound field is dominated by scattered modes—the mode spacing is 8 equal to the number of splices. At low supersonic fan speeds, the measured levels of the scattered modes were higher than the rotor-alone component of the pressure field. However, at higher supersonic fan speeds the measured levels of the rotor-alone modes were significantly higher, and exceeded the level of any scattered modes in the inlet duct. These findings are examined in this article.

One of the main objectives of most of this previous work was to examine the potential benefit of using circumferentially varying liners to increase attenuation of sound. There has been less work directly applicable to current turbofan engines, and the scattering caused by discontinuities in the acoustic lining. The

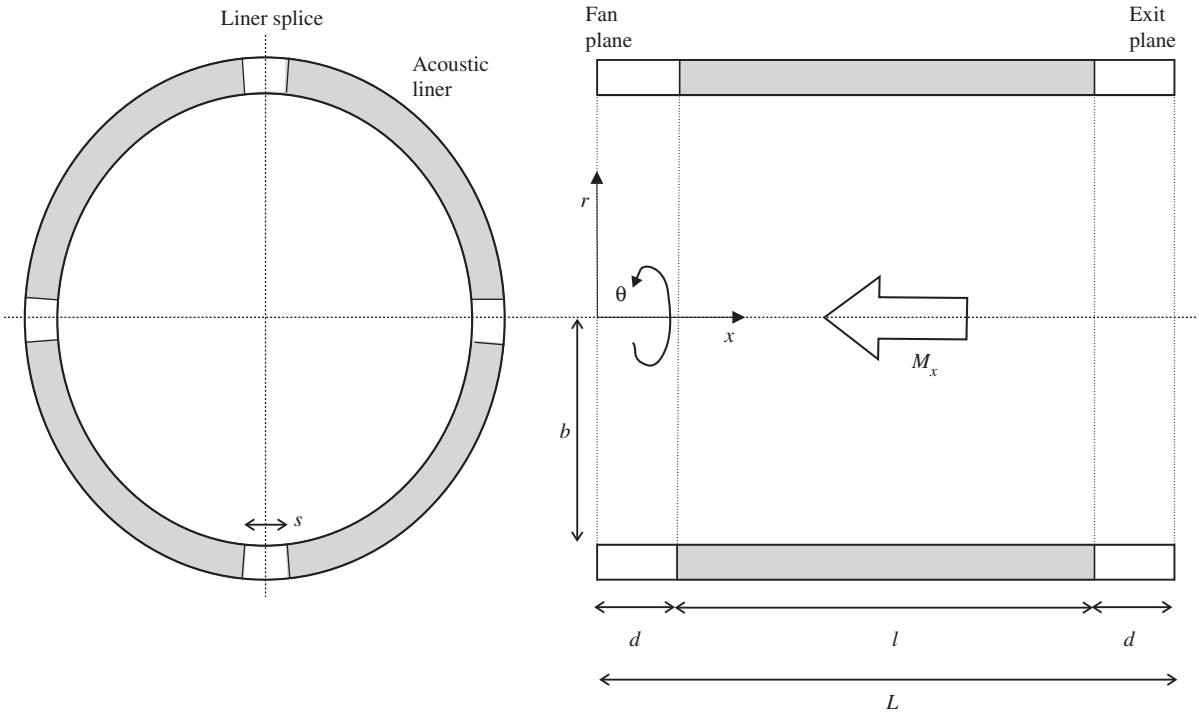

Fig. 1. Inlet duct geometry.

objective of this article is to assess the acoustic scattering by splices (of different widths), at supersonic fan speeds, in a lined inlet duct. Also, the noise benefit that a uniform lining with no splices could provide is examined.[1]

2. Scattering by liner splices

A turbofan inlet duct can be modelled approximately by a circular-section cylindrical duct. An approximate inlet duct geometry is shown sketched in Fig. 1. Take cylindrical polar coordinates (r, θ, x) such that the centre of the duct is aligned with the x-axis, the fan plane is at $x = 0$, the exit plane is at $x = L$, and the duct wall is at $r = b$. The duct is lined from $x = d$ to $d + l$. The acoustic lining contains N_s axial splices, each of width s, positioned $2\pi/N_s$ radians apart around the duct's circumference. Also, the duct contains a uniform mean flow $\mathbf{u}_0 = U_0\hat{\mathbf{x}}$, with Mach number $M_x = U_0/c_0$.

The sound field in a waveguide or duct is commonly expressed in terms of modes. It is convenient to consider fan tones generated by a turbofan engine in terms of spinning modes (based on a circular-section cylindrical duct). Assume that inside the duct, a harmonic noise source with frequency ω generates a harmonic pressure field, $p'(r, \theta, x, t) = \hat{p}(r, \theta, x)\exp(\mathrm{i}\omega t)$, which is determined by solving the convected Helmholtz equation,

$$\left(\mathrm{i}k + M_x \frac{\partial}{\partial x}\right)^2 \hat{p} = \nabla^2 \hat{p}, \quad k = \omega/c_0. \tag{1}$$

[1]Some of the work in this article was presented at the 10th AIAA/CEAS Aeroacoustics Conference, see Ref. [13], Part I: Finite Element Assessment.

It is well known (e.g. as shown by Eversman [14]), that on separating the variables r, θ and x the acoustic pressure can be expressed as a Fourier–Bessel modal sum

$$\begin{aligned}\hat{p}(r,\theta,x) &= \sum_{m=-\infty}^{\infty}\sum_{n=1}^{\infty}(\hat{p}^{+}_{m,n}+\hat{p}^{-}_{m,n})\\ &= \sum_{m=-\infty}^{\infty}\sum_{n=1}^{\infty}(A^{+}_{m,n}J_m(\kappa^{+}_{m,n}r)\mathrm{e}^{\mathrm{i}(m\theta-k_{x^{+}_{m,n}}x)}+A^{-}_{m,n}J_m(\kappa^{-}_{m,n}r)\mathrm{e}^{\mathrm{i}(m\theta-k_{x^{-}_{m,n}}x)}),\end{aligned} \tag{2}$$

where

$$k_{x^{\pm}_{m,n}}=\frac{k}{1-M_x^2}\left(-M_x\pm\sqrt{1-(1-M_x^2)\left(\frac{\kappa^{\pm}_{m,n}}{k}\right)^2}\right). \tag{3}$$

Each mode is identified by its azimuthal and radial order, m and n, denoted by subscript m,n. Note that $+,-$ denote right- and left-running modes, respectively.

In a rigid-walled duct, at a fixed frequency, only a finite number of modes can propagate inside the duct and transmit acoustic power. The number of propagating, or "cut-on", modes in a duct depends upon the frequency ω, the duct radius b, and the mean flow M_x. All the remaining modes will be "cut-off" and transmit no acoustic power. Mode (m,n) will be a propagating mode if its cut-off ratio $\zeta_{m,n}>1$, where

$$\zeta_{m,n}=\frac{kb}{\kappa_{m,n}b\sqrt{1-M_x^2}}. \tag{4}$$

If $\zeta_{m,n}>1$, then the axial decay rate $\mathrm{Im}\{k_{xm,n}\}$ is zero.

In an acoustically lined duct, the acoustic pressure also can be expressed by a Fourier–Bessel modal sum (similar to Eq. (2)), but with different modal amplitudes $A^{\pm}_{m,n}$, and $\kappa^{\pm}_{m,n}$, $k_{x^{\pm}_{m,n}}$ replaced with $\mu^{\pm}_{m,n}$, $\alpha_{x^{\pm}_{m,n}}$, to distinguish between rigid and lined duct modes. (All the values of μ and α_x are complex.) It will be useful to extend the normal use of the terms 'cut-on' and 'cut-off' also to describe modes in a lined duct. Modes which are cut-off ($\zeta<1$), or near cut-off ($\zeta\approx 1$), typically are well absorbed by an acoustic lining. At higher values of ζ (greater than one), the modes are more cut-on, and tend to be poorly absorbed by an acoustic lining. For a fixed azimuthal mode order m, $\zeta_{m,1}>\zeta_{m,2}>\zeta_{m,3},\ldots$, so in a lined duct, typically the axial decay rates, $\mathrm{Im}\{\alpha_{xm,1}\}<\mathrm{Im}\{\alpha_{xm,2}\}<\mathrm{Im}\{\alpha_{xm,3}\},\ldots$, and $(m,1)$ is the least attenuated mode.

At supersonic fan speeds, the rotor-alone pressure field can be modelled by modes spinning with the same circumferential phase speed as the fan, which equals $2\pi\mathscr{F}$. The circumferential phase speed of a spinning mode is ω/m. Therefore, a rotor-alone tone with frequency $m\times\mathscr{F}$ can be modelled by spinning modes with azimuthal mode order m. The rotating fan's circumferential phase speed will be supersonic only over a small spanwise section of the blade, close to the blade's tip. It follows that at the fan plane most of the acoustic energy will be contained in modes with radial mode order $n=1$. This means that the fan tonal noise source can be modelled, at frequency $m\mathscr{F}$, by the rotor-alone mode $(m,1)$.

First, consider the sound power transmission loss in a uniformly lined duct with no splices. At each junction between the rigid and lined duct sections there is acoustic scattering, caused by the change in impedance at the wall. Energy is scattered between different modes. However, because the lining is uniform (axisymmetric problem), for a given azimuthal mode order m, the scattering will be only between different radial modes. With no liner splices, the transmitted modes at the exit plane will be $(m,1)$, $(m,2)$, $(m,3)$, etc.

The modal sound power $W^{\pm}_{m,n}$ is given by

$$W^{\pm}_{m,n}=2\pi\int_{r=0}^{b}I_{x^{\pm}_{m,n}}r\,\mathrm{d}r, \tag{5}$$

i.e. the integral of the modal acoustic intensity $I_{x^{\pm}_{m,n}}$ in the $\pm x$-direction over the cross-sectional area of the duct. The form of the axial acoustic intensity is given by Morfey ([15, Eq. (16), p. 39]). This leads to

$$W^{\pm}_{m,n}=|A^{\pm}_{m,n}|^2\chi^{\pm}_{m,n}, \tag{6}$$

where

$$\chi^{\pm}_{m,n} = \frac{\pi b^2}{2\rho_0 c_0} |J_m(\kappa_{m,n} b)|^2 \left[1 - \left(\frac{m}{\kappa_{m,n} b}\right)^2\right] \left[(1 + M_x^2)\,\mathrm{Re}\{\xi^{\pm}_{m,n}\} + M_x(1 + |\xi^{\pm}_{m,n}|^2)\right] \tag{7}$$

and

$$\xi^{\pm}_{m,n} = \frac{k_{x^{\pm}_{m,n}}}{k - k_{x^{\pm}_{m,n}} M_x}. \tag{8}$$

At the fan and exit planes, as the duct wall is rigid, the power in each mode can be summed because the mode shapes are orthogonal. Thus, here the sound power transmission loss, at frequency equal to $m\mathscr{F}$, is defined as

$$\Delta_{\mathrm{PWL}} = 10 \log_{10} \left(W^{+}_{m,1}\big|_{\text{fan plane}} \Big/ \sum_{n=1}^{n_c(m)} W^{+}_{m,n}\big|_{\text{exit plane}} \right) \mathrm{dB}. \tag{9}$$

In the absence of liner splices, at a fixed azimuthal mode order m, acoustic energy can be only scattered into higher radial mode orders, which will be nearer cut-off. Therefore, the main factor which determines the transmission loss in the lined duct section will be the axial decay rate of the least attenuated mode, which is assumed to be mode $(m, 1)$. Hence, a simpler estimate of the transmission loss is defined as,

$$\Delta_{\mathrm{LAM}} = -20\,\mathrm{Im}\{\alpha_{x^{+}_{m,1}}\} l \log_{10} \mathrm{e}, \tag{10}$$

which is based on the least attenuated right-running mode.

Now consider the sound power transmission loss in a uniformly lined duct with N_s splices each of width s. In principle, the acoustic pressure can be expressed as

$$\hat{p}(r, \theta, x) = \sum_{l=1}^{\infty} A^{+}_{l} \psi^{+}_{l}(r, \theta) \mathrm{e}^{\mathrm{i}(-\alpha_{x^{+}_{l}} x)} + A^{-}_{l} \psi^{-}_{l}(r, \theta) \mathrm{e}^{\mathrm{i}(-\alpha_{x^{-}_{l}} x)}, \tag{11}$$

where the mode shapes $\psi_l(r, \theta)$ describe the acoustic field over a cross-sectional plane of the duct (see Refs. [4–6]).

Scattering caused by liner splices can be significant because energy is scattered into different azimuthal and radial mode orders. The transmitted modes will be comprised of azimuthal mode orders $im \pm jN_s$, where i, j are integers. These scattered modes are directly analogous to rotor–stator interaction modes, which Tyler and Sofrin [1] showed are given by $m = iB \pm jV$.

As before, assume that the incident mode at the fan plane is the rotor-alone mode $(m, 1)$. Energy will be scattered into azimuthal mode orders $im \pm jN_s$. The scattered modes with $|im \pm jN_s| < |m|$ will rotate with a faster circumferential phase speed than the fan. The cut-off ratios of these scattered modes will be greater than $\zeta_{m,1}$, so typically these scattered modes will be less well absorbed by the acoustic liner, compared with the original rotor-alone mode.

Now the sound power transmission loss is defined as

$$\Delta_{\mathrm{PWL}} = 10 \log_{10} \left(W^{+}_{m,1}\big|_{\text{fan plane}} \Big/ \sum_{m=-m_c}^{m_c} \sum_{n=1}^{n_c(m)} W^{+}_{m,n}\big|_{\text{exit plane}} \right) \mathrm{dB}. \tag{12}$$

Compare Eqs. (9) and (12). With a spliced liner, if the rotor-alone modes are near cut-off, and well absorbed by the acoustic lining, then at the exit plane the sound field is likely to be dominated by the non-rotor-alone modes, that are generated by scattering caused by the splices.

3. Finite-element method

The acoustic field in the inlet duct was simulated using ACTRAN/AE, a finite/infinite-element code produced by Free Field Technologies.[2]

[2]Free Field Technologies S.A., 16 place de l'Université, B-1348 Louvain-la-Neuve, Belgium. http://www.fft.be, info@fft.be.

The flow acoustic model is based on an irrotational mean flow. The fluid is a non-viscous, non-heat conducting, perfect gas. It can be described by the following equations:

$$\text{Continuity}: \quad \frac{\partial \rho}{\partial t} + \nabla \cdot (\rho \mathbf{u}) = 0, \tag{13}$$

$$\text{Momentum}: \quad \frac{\partial \mathbf{u}}{\partial t} + (\mathbf{u} \cdot \nabla)\mathbf{u} = -\frac{1}{\rho}\nabla p, \tag{14}$$

$$\text{Equation of state}: \quad p = p_0 \left(\frac{\rho}{\rho_0}\right)^{\gamma}. \tag{15}$$

The velocity $\mathbf{u}$ can be expressed in terms of a velocity potential ϕ, where

$$\mathbf{u} = \nabla \phi, \tag{16}$$

because the flow is irrotational. Acoustic disturbances in the flow can be described by decomposing the velocity potential

$$\phi(\mathbf{x}, t) = \phi_0(\mathbf{x}) + \phi'(\mathbf{x}, t). \tag{17}$$

The steady-state mean flow is given by

$$\mathbf{u}_0 = \nabla \phi_0, \tag{18}$$

where it is assumed that the acoustic velocity potential $\phi' \ll \phi_0$.

Harmonic acoustic disturbances are given by

$$\phi'(\mathbf{x}, t) = \hat{\phi}(\mathbf{x})\, \mathrm{e}^{\mathrm{i}\omega t}. \tag{19}$$

On combining Eqs. (13)–(15), $\hat{\phi}(\mathbf{x})$ is found by solving the convected Helmholtz equation

$$\mathrm{i}\omega \left(\frac{\rho_0}{c_0^2}[\mathrm{i}\omega + \mathbf{u}_0 \cdot \nabla]\hat{\phi}\right) - \nabla \cdot \left(\rho_0 \nabla \hat{\phi} - \frac{\rho_0}{c_0^2}\mathbf{u}_0[\mathrm{i}\omega + \mathbf{u}_0 \cdot \nabla]\hat{\phi}\right) = 0. \tag{20}$$

Note that for uniform flow, $\mathbf{u}_0 = U_0 \hat{\mathbf{x}}$, and Eq. (20) reduces to

$$\left(\mathrm{i}\omega + U_0 \frac{\partial}{\partial x}\right)^2 \hat{\phi} = c_0^2 \nabla^2 \hat{\phi}, \tag{21}$$

which is equivalent to Eq. (1).

The FE method is based on a weak variational statement constructed by multiplying Eq. (20) by weight function $\delta\hat{\phi}$, and integrating over the acoustic domain Ω:

$$\int_\Omega \rho_0 \left(\nabla \hat{\phi} \cdot \nabla \delta\hat{\phi} - \left(\frac{\mathbf{u}_0}{c_0} \cdot \nabla \hat{\phi}\right)\left(\frac{\mathbf{u}_0}{c_0} \cdot \nabla \delta\hat{\phi}\right)\right) \mathrm{d}\Omega \tag{22}$$

$$+ \mathrm{i}\omega \int_\Omega \frac{\rho_0}{c_0^2}\left(\delta\hat{\phi}(\mathbf{u}_0 \cdot \nabla \hat{\phi}) - \hat{\phi}(\mathbf{u}_0 \cdot \nabla \delta\hat{\phi})\right) \mathrm{d}\Omega - \omega^2 \int_\Omega \frac{\rho_0}{c_0^2}\, \hat{\phi}\, \delta\hat{\phi}\, \mathrm{d}\Omega$$

$$= \int_\Gamma \delta\hat{\phi}\left(\rho_0 \nabla \hat{\phi} - \frac{\rho_0}{c_0^2}\left[\mathrm{i}\omega\hat{\phi} + \mathbf{u}_0 \cdot \nabla \hat{\phi}\right]\mathbf{u}_0\right) \cdot \hat{\mathbf{n}}\, \mathrm{d}\Gamma. \tag{23}$$

The surface integral in Eq. (23) can be simplified because it is assumed that on Γ the mean flow is tangent to the boundary surface, so $\mathbf{u}_0 \cdot \hat{\mathbf{n}} = 0$. Also $\nabla\hat{\phi} \cdot \hat{\mathbf{n}} = \hat{u}_n$, where $\hat{u}_n \exp(\mathrm{i}\omega t)$ is the acoustic particle velocity on Γ (directed outwards). The surface integral is then calculated by using the impedance boundary condition originally derived by Myers [16]:

$$\mathrm{i}\omega\hat{u}_n = \{\mathrm{i}\omega + \mathbf{u}_0 \cdot \nabla - \mathbf{n} \cdot (\mathbf{n} \cdot \nabla \mathbf{u}_0)\}\left(\frac{1}{\rho_0 c_0}\frac{\hat{p}}{Z}\right) \quad \text{on } \Gamma. \tag{24}$$

In general, the acoustic domain Ω is divided into an inner and outer domain. (Infinite elements are used for the outer domain.) However, in this case only an inner domain is required. Conventional Galerkin FEs are

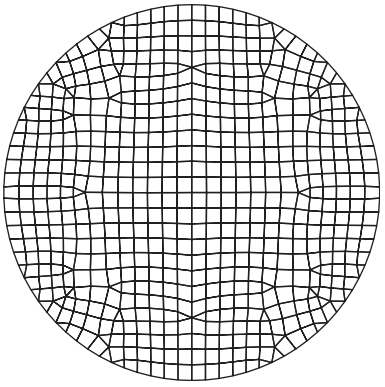

Fig. 2. A typical cross-sectional mesh.

used to discretize the acoustic domain. These take the form

$$\hat{\phi}(\mathbf{x}) = \sum_i \hat{\phi}_i \mathcal{N}_i(\mathbf{x}), \tag{25}$$

where $\hat{\phi}_i$ is the value of $\hat{\phi}$ at the ith node point, and $\mathcal{N}_i$ are the basis functions for each FE. The Galerkin method uses these basis functions for the weight functions. This leads to a matrix equation which replaces Eq. (23). The matrix equation is usually written in the form

$$(-\omega^2[\mathbf{M}] + \mathrm{i}\omega[\mathbf{C}] + [\mathbf{K}])\mathbf{\Phi} = \mathbf{F}, \tag{26}$$

where [**M**], [**C**] and [**K**] are referred to as the mass, damping and stiffness matrices, respectively, $\mathbf{\Phi}$ is a vector whose ith element is $\hat{\phi}_i$, and **F** is the force vector (determined by the boundary condition on Γ). Full details of the FE procedure can be found in the ACTRAN user manual [17].

The ACTRAN/AE mesh was generated using the ICEM[3] CFD 4.1 package. The cross-section was meshed with a mixture of quadrilateral and triangular elements with a resolution of eight nodes per wavelength λ. All the elements are quadratic. A typical cross-sectional mesh is shown in Fig. 2. This mesh was then extruded along the duct, with the depth of each layer being such that the axial resolution was ten nodes per wavelength, when reduced by a factor of $(1 - M_x)$ to account for the effect of flow.

The mean flow $\mathbf{u}_0$ is calculated separately, and then interpolated onto the mesh used by ACTRAN/AE. In this case the mean flow is uniform, so no extra calculation of the flow, (using for example a CFD code), was required.

A particular feature of ACTRAN/AE, which makes it suitable for this type of duct acoustics problem, is that duct boundary conditions can be specified in terms of modes. The fan and exit planes are shown in Fig. 1. At each plane, modes propagating in either direction can be specified to be fixed (at a particular amplitude) or free.

At the fan plane, the amplitudes of the right-running incident modes are specified, and all the left-running reflected modes are free. At the exit plane, all the right-running transmitted modes are free; no left-running modes were specified, corresponding to an anechoic termination. The number of modes used was specified, the criterion being that modes whose cut-off ratio $\zeta > 0.9$ were included. This means that some evanescent modes will be included; these will be modes which decay axially but sufficiently slowly that they may be significant due to the short distance d between the fan, or exit plane, and the liner.

A post-processing routine was used to calculate the modal sound powers from the amplitudes of the transmitted and reflected waves. As discussed in Section 2, the transmitted power can be determined by summing the power in all the cut-on modes because the mode shapes are orthogonal.

[3] http://www.icemcfd.co.uk/

The method was calibrated by comparing results for a uniform lining with no splices against results from a mode-matching procedure. This validation test case is included in the results, see Section 5. (Full details of the mode-matching procedure will be included in a subsequent article on acoustic scattering by an axially segmented liner.)

The only other similar FE calculations for a turbofan inlet duct liner appear to be by Regan and Eaton [18]. Their results demonstrate the suitability of using the FE method for modelling sound transmission in a lined inlet duct containing splices.

This type of FE method tends to scale poorly with frequency, prohibiting its use at high frequencies. In a real turbofan engine the non-dimensional frequency kb of the BPF tone, at supersonic fan speeds, is likely to be between 30 and 40. Three-dimensional FE simulations at realistic BPFs are extremely costly, both in CPU time and memory.[4] In this article, in order to reduce the computational cost, a model-scale problem is examined. Numerical simulations of acoustic scattering and transmission in a three-dimensional lined duct have been conducted at a kb corresponding to about $\frac{1}{2}$BPF. The aim is to use a model-scale problem that preserves most of the physics of the original (full-scale) problem, so that meaningful results applicable to a real turbofan engine can be obtained from computations at a reduced frequency.

4. Specification of the problem

A heuristic scaling procedure is proposed in order to reduce the Helmholtz number kb used in the FE simulations. A model-scale (reduced frequency) problem is used to simulate realistic supersonic fan operating conditions, the aim being to preserve most of the physics of the full-scale problem.

The scattering and transmission of sound in a lined turbofan inlet duct containing splices is modelled by using the inlet duct geometry shown in Fig. 1. The values of the parameters used in this analysis are listed in Table 1. These values are realistic for a modern high-bypass-ratio turbofan aero-engine.

Table 2 lists the details of the two supersonic fan speeds, "cut-back" and "sideline", used in this analysis. The maximum rpm (100% fan speed) is 4600. Thus $M_t > 1$ at fan speeds above 70%. The nominal "cut-back" and "sideline" fan speeds are close to 80% and 90%. The incident sound field is modelled, at frequency $m \times \mathscr{F}$, by the rotor-alone mode $(m, 1)$. The values of BPF $(B \times \mathscr{F})$, and the cut-off ratio of mode $(B, 1)$, at cut-back and sideline, also are listed in Table 2.

The acoustic liner is a locally reacting single-layer cavity lining. The non-dimensional specific acoustic impedance[5] of the lining is

$$Z = R + \mathrm{i}X. \tag{27}$$

The values of Z used in this analysis are $2.50 + 0.57\,\mathrm{i}$ at cut-back, and $3.00 + 1.00\,\mathrm{i}$ at sideline. The resistance R is taken to be independent of the frequency. Realistic values of R are specified. The reactance X is dependent on the frequency, so values for BPF are specified. At cut-back, the cut-off ratio of mode $(B, 1)$ is $\zeta_{B,1} = 1.10$, so as the mode is near cut-off, it should be well absorbed by the lining. At sideline, mode $(B, 1)$ should be less well absorbed by the lining, as its cut-off ratio is $\zeta_{B,1} = 1.36$. Thus, values of X are specified, so that for a uniform lining (with no splices), Δ_{LAM} is about 40 dB at cut-back, and about 10 dB at sideline. This is a realistic difference in the values of the transmission loss at cut-back and sideline.

In terms of the acoustic pressure, a reduction of 40 dB means that the pressure is reduced by a factor of 100. With a transmission loss of up to 40 dB, the correct modal amplitudes at the exit plane could be determined from the FE simulations. In principle, acoustic energy should only be scattered into azimuthal mode orders $im \pm jN_s$. Using the FE method, a small amount of energy is scattered (by the numerical scheme) into other mode orders. The amplitudes of these modes will be much lower than the amplitudes of the liner scattered modes, unless the transmission loss is significantly larger than 40 dB, in which case it may be difficult to resolve the correct levels at the exit plane.

[4]In Ref. [18] there is only one computation at a frequency close to that generated by a real turbofan (at $kb = 20$).

[5]The acoustic impedance has been non-dimensionalized by dividing by $\rho_0 c_0$ ($c_0 = 340\,\mathrm{ms}^{-1}$ and $\rho_0 = 1.2\,\mathrm{kg\,m}^{-3}$).

Table 1
Inlet duct specification (full-scale problem)

Number of fan blades	B	24
Duct radius	b	1.0 m
Duct length	L	1.1 m
Liner length	l	0.8 m
Rigid-walled section	d	0.15 m
Number of splices	N_s	4
Splice width	s	0, 20, 30, 40, 50, 60 mm

Table 2
Fan operating conditions (full-scale problem)

Fan speed	M_x	M_t	BPF (Hz)	kb	$\zeta_{B,1}$
Cut-back	−0.40	1.11	1440	26.6	1.10
Sideline	−0.50	1.29	1680	31.0	1.36

So, the prescribed values of the reactance also were selected because this should ensure that the maximum transmission loss would not exceed 40 dB for any of the spliced liner simulations. Note that this means the prescribed values of Z are not equal to the Cremer optimum impedance.

The model-scale problem is specified as follows. The key step is to halve the number of fan blades, i.e. $B \to B^\star = \frac{1}{2}B$,[6] and to reduce the fan rpm speed such that the cut-off ratio of the BPF mode $(B, 1)$ is the same at full and model scale. This approximately halves BPF at model scale. Preserving $\zeta_{B,1}$ is crucial to ensure that the attenuation at full and model scale are about the same.

In the model-scale problem s, N_s and Z are also changed. The splice width s is increased such that ks is preserved. This ensures that the effect of changing the splice width can be predicted at model scale. The number of splices N_s is also halved, i.e. $N_s \to N_s^\star = \frac{1}{2}N_s$. This ensures that the ratio of rotor-alone to scattered azimuthal mode order, $B/(B \pm jN_s)$, is preserved.

A different acoustic impedance is used at model scale, the aim being to adjust the impedance from Z to $Z^\star$, so that *if* the lining is uniform with no splices, then the decay of mode $(B, 1)$ would be the same at full and model scale. The new acoustic impedance is determined by searching the complex impedance plane, to find $Z^\star$ such that the axial phase speed and axial decay rate of mode $(B, 1)$ are matched. This requires $\mathrm{Re}\{\alpha_{x\,B,1}^{+}/k\}$ and $\mathrm{Im}\{\alpha_{x\,B,1}^{+}\}$ to be matched at full and model scale.

The remaining variables b, M_x, L and l are unchanged. This ensures that the mass flow in the full- and model-scale problem is the same. A comparison of the inlet ducts used at full and model scale are shown sketched in Fig. 3.

It is assumed that there exists a suitable impedance $Z^\star$ to be used at model scale. The choice of $Z^\star$ is based on the axial wavenumber $\alpha_{x\,B,1}$ for a uniformly lined duct, because in practice the axial wavenumbers for a spliced liner in Eq. (11) are not known. The equivalent value of α_x, for the rotor-alone component of the pressure field in a lined duct containing splices, is assumed to be similar to $\alpha_{x\,B,1}$. The inherent assumption is that splices cause scattering, but that this does not significantly alter the structure of the rotor-alone component of the acoustic pressure field.

A suitable value of $Z^\star$ is found by searching the complex impedance plane to minimize

$$h = \sqrt{(\mathrm{Re}\{\alpha_{x\,B,1}^{+}/k - \alpha_{x\,B,1}^{+\,\star}/k^\star\})^2 + (\mathrm{Im}\{\alpha_{x\,B,1}^{+} - \alpha_{x}^{+\star}{}_{B,1}\})^2}. \tag{28}$$

Figs. 4 and 5 are contour plots of $-\log_{10} h$ in the $Z = (R, X)$-plane, at the cut-back and sideline fan speeds, respectively. In each case, an impedance to use for the model-scale problem is located.

[6]Note that * denotes the value at model scale.

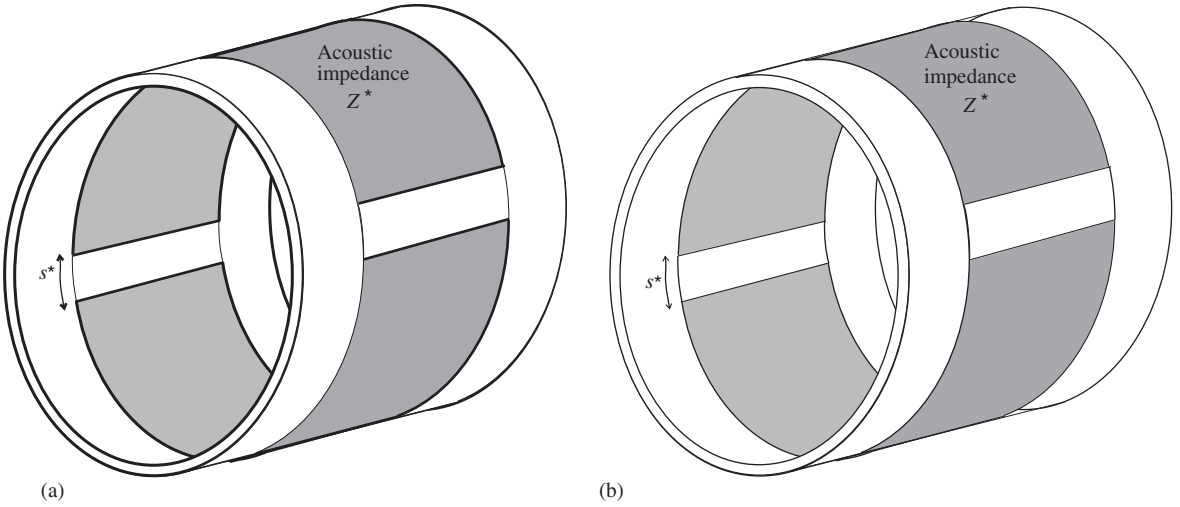

Fig. 3. (a) Full- and (b) model-scale inlet duct.

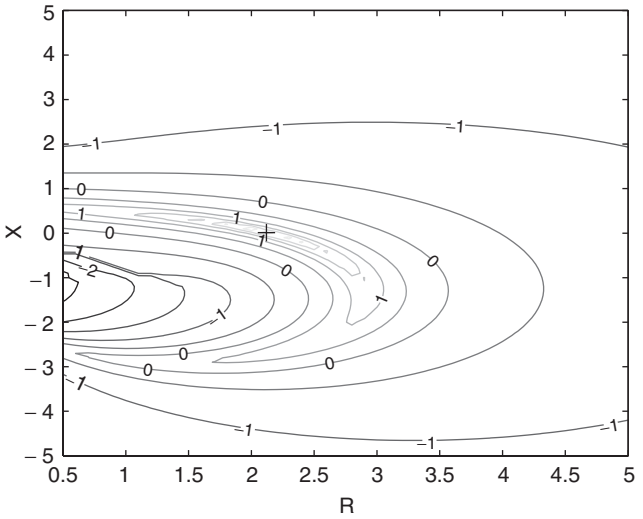

Fig. 4. Model-scale results. Contour plot of $-\log_{10} h$ in (R, X)-plane—cut-back fan speed. Model-scale impedance $Z^\star = 2.12 + 0.01\,\mathrm{i}$ (+).

In this article results of FE simulations of liner scattering, at supersonic fan speeds, are examined. The simulations are conducted at a reduced BPF, by halving the number of fan blades. In light of this, the following results and discussion (Sections 5 and 6), apply to the model-scale problem. How well the results at model scale compare with at full scale is discussed in Appendix A.

5. Results

The results in this article show predictions of the attenuation of fan tone noise by a spliced liner. The two principal objectives of this study are to investigate how the attenuation is affected by: (1) fan speed; (2) splice width. Also, the aim is to assess the potential noise benefit that could be gained by manufacturing a uniform acoustic lining with no splices. At the cut-back and sideline fan speeds, the scattering and transmission of the BPF mode $(B, 1)$ is simulated, for an inlet duct containing a uniform lining with no splices, and a uniform lining with splices of width $s = 20-60\,\mathrm{mm}$ (full-scale values).

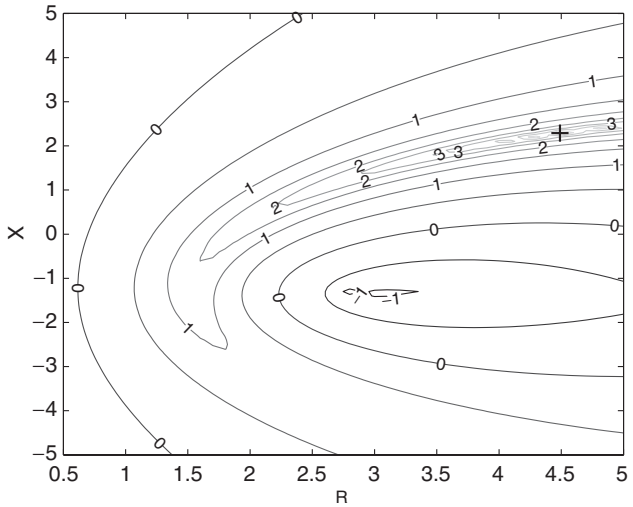

Fig. 5. Model-scale results. Contour plot of $-\log_{10} h$ in (R, X)-plane—sideline fan speed. Model-scale impedance $Z^{\star} = 4.49 + 2.29\mathrm{i}$ (+).

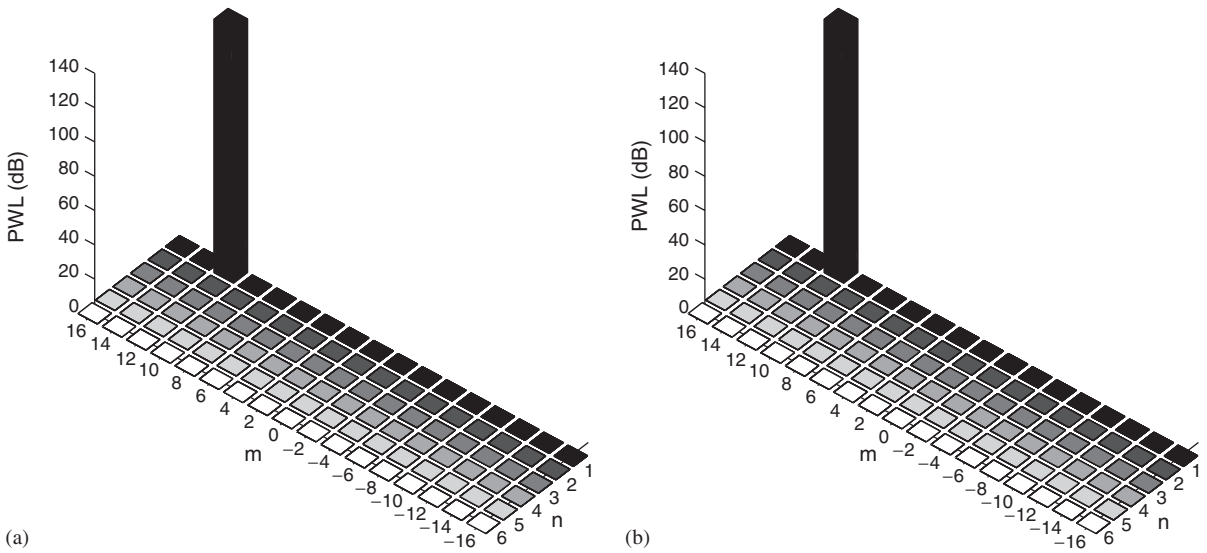

Fig. 6. Model-scale results. Sound power level of right-running incident modes at the fan plane. (a) Cut-back and (b) sideline.

In all the simulations, at the fan plane the prescribed sound power of the right-running incident mode $(B, 1)$ is 147.8 dB, see Fig. 6.[7] At full scale, this corresponds to an equivalent sound pressure level (SPL) of 170 dB, which is a realistic level of the BPF tone.

In Fig. 7, the effect of scattering by the liner splices, is shown for several different examples. In each case, the predicted sound powers of *all* the right-running modes at the exit plane are shown. Then, in Figs. 8 and 9, the variation of the azimuthal modal sound powers with splice width, at the cut-back and sideline fan speeds, are shown. Comparison of Figs. 8 and 9 illustrates two important findings: how the results change at different fan speeds, and how the scattering is affected by the width of the splices. This is also shown in Fig. 10 which plots how each azimuthal modal sound power level varies with splice width, at the two supersonic fan speeds.

[7]Absolute levels are shown.

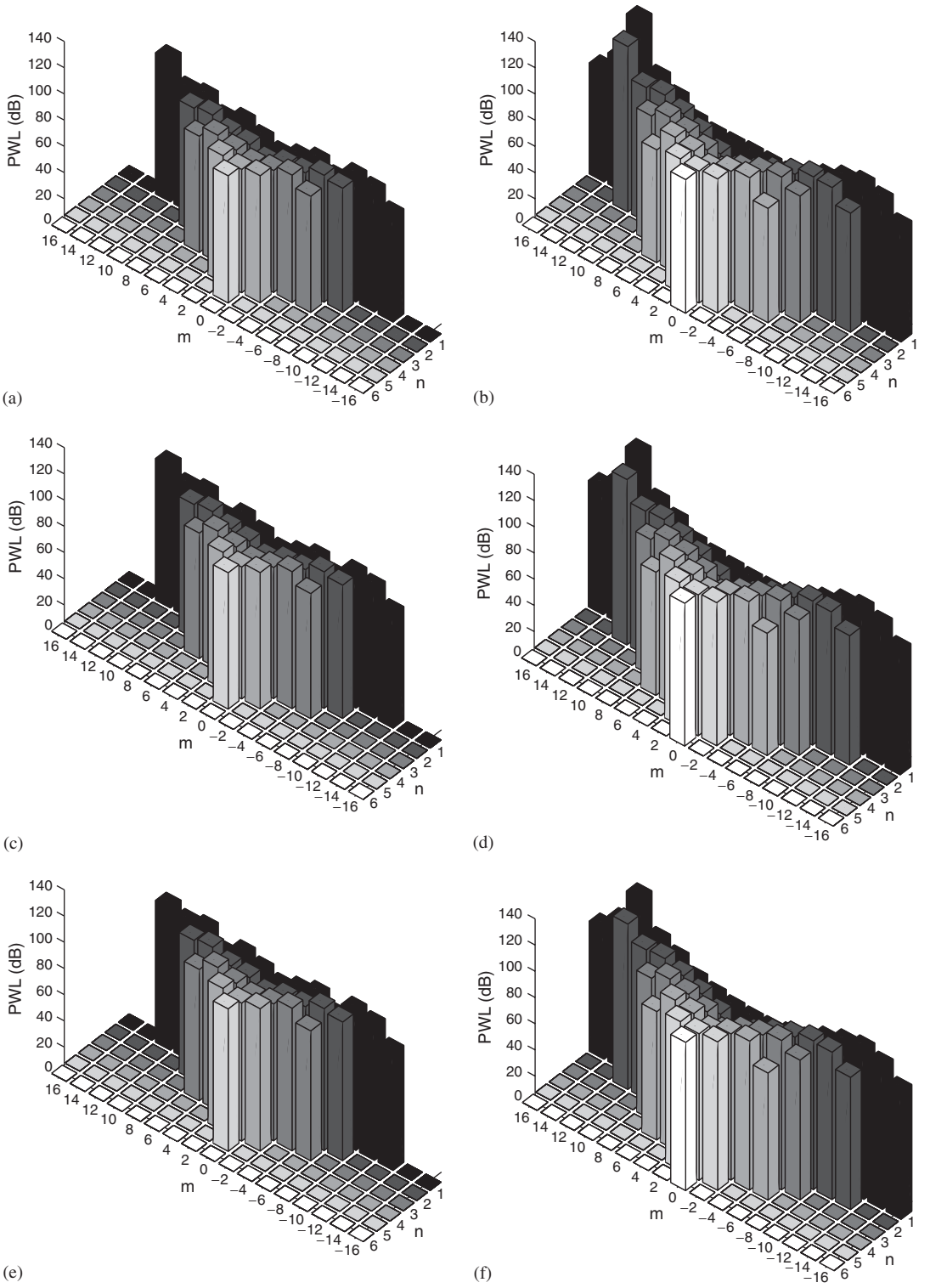

Fig. 7. Model-scale results. Sound power level of right-running transmitted modes at the exit plane. (a) Cut-back—splice width = 20 mm, (b) sideline—splice width = 20 mm, (c) cut-back—splice width = 40 mm, (d) sideline—splice width = 40 mm, (e) cut-back—splice width = 60 mm and (f) sideline—splice width = 60 mm.

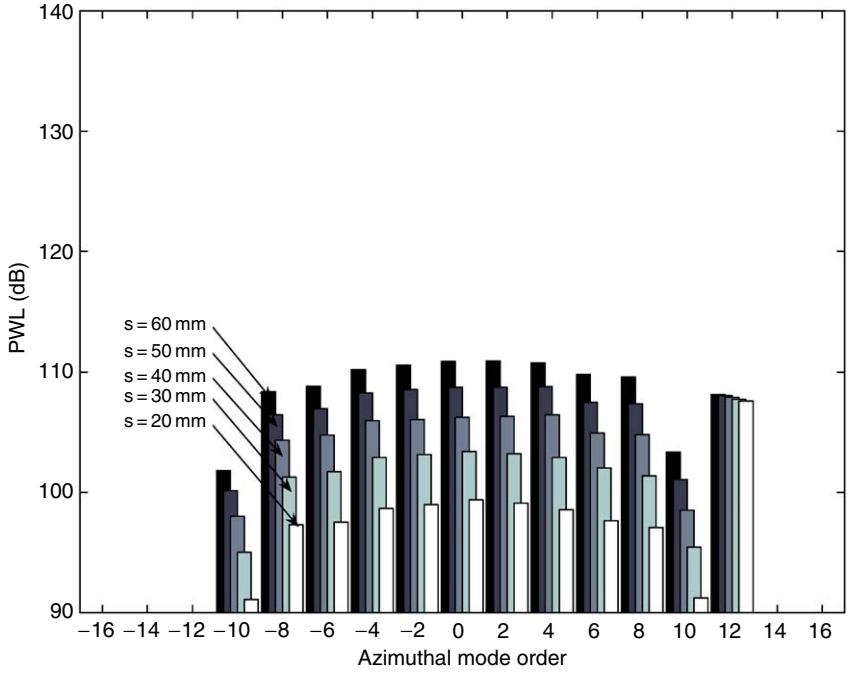

Fig. 8. Model-scale results. Sound power levels at the exit plane—cut-back fan speed. Results are shown for different splice widths.

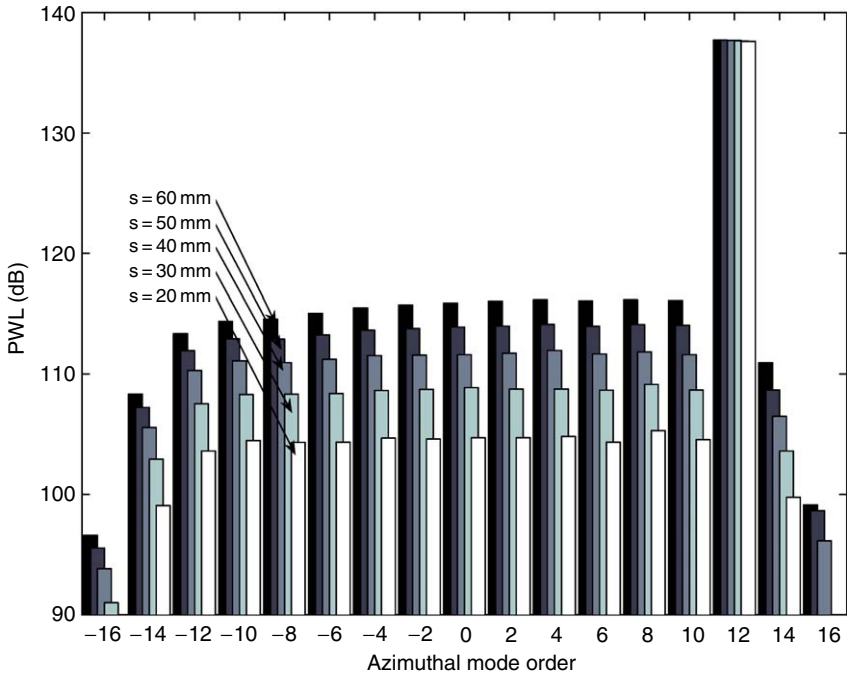

Fig. 9. Model-scale results. Sound power levels at the exit plane—sideline fan speed. Results are shown for different splice widths.

Finally, in Fig. 11 the variation in sound power transmission loss with splice width is shown, at the cut-back and sideline fan speeds. The values of Δ_{PWL} are also listed in Table 3. This includes the case of a uniform lining with no splices ($s = 0$ mm). Note that with a uniform liner, there is close agreement between the FE and mode-matching results. The example of a zero thickness splice has been used to check the accuracy of the FE code.

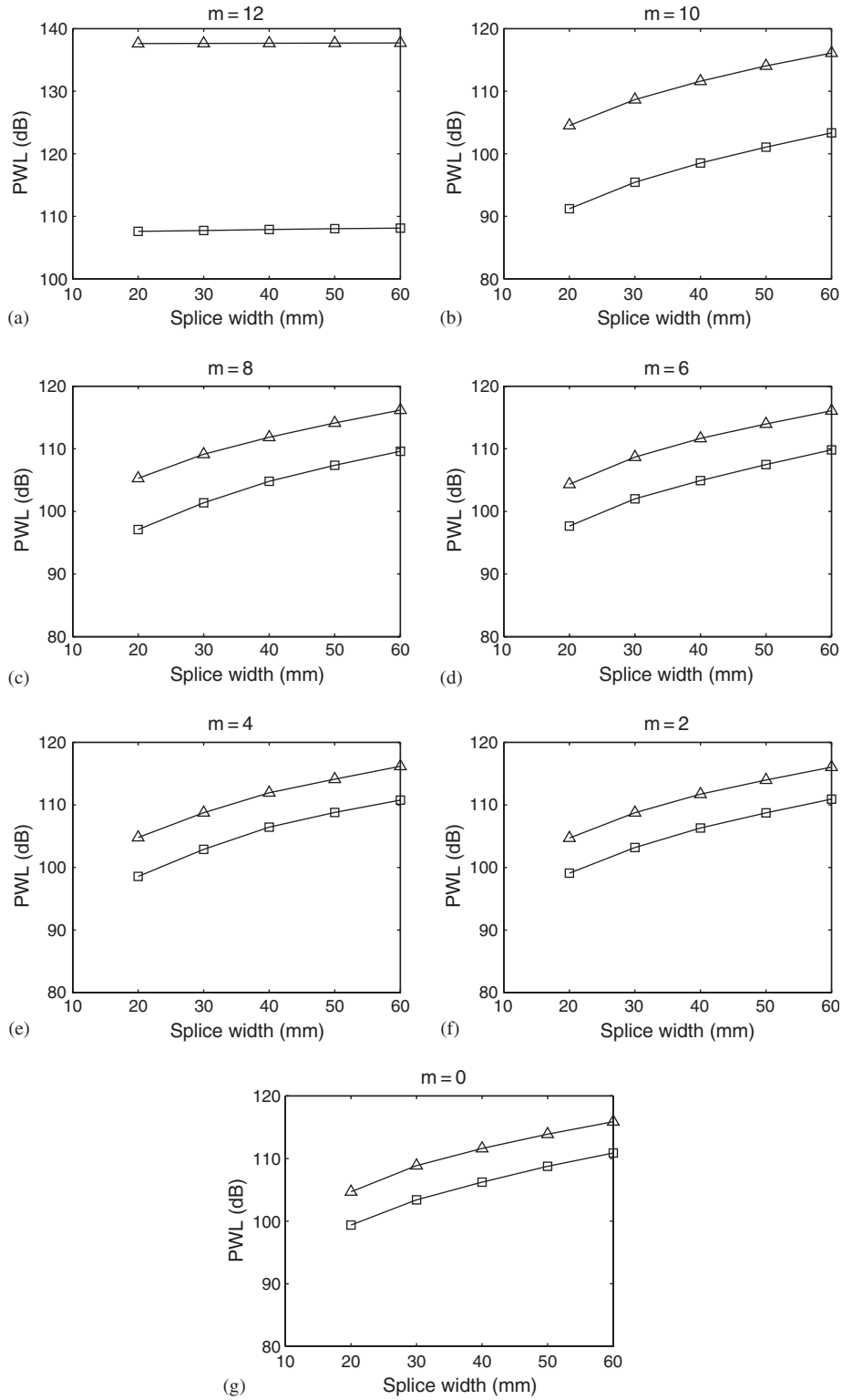

Fig. 10. Model-scale results. Variation in sound power levels at the exit plane with different splice widths. Azimuthal mode orders (a) $m = 12$ to (g) $m = 0$. Key: □, cut-back; △, sideline.

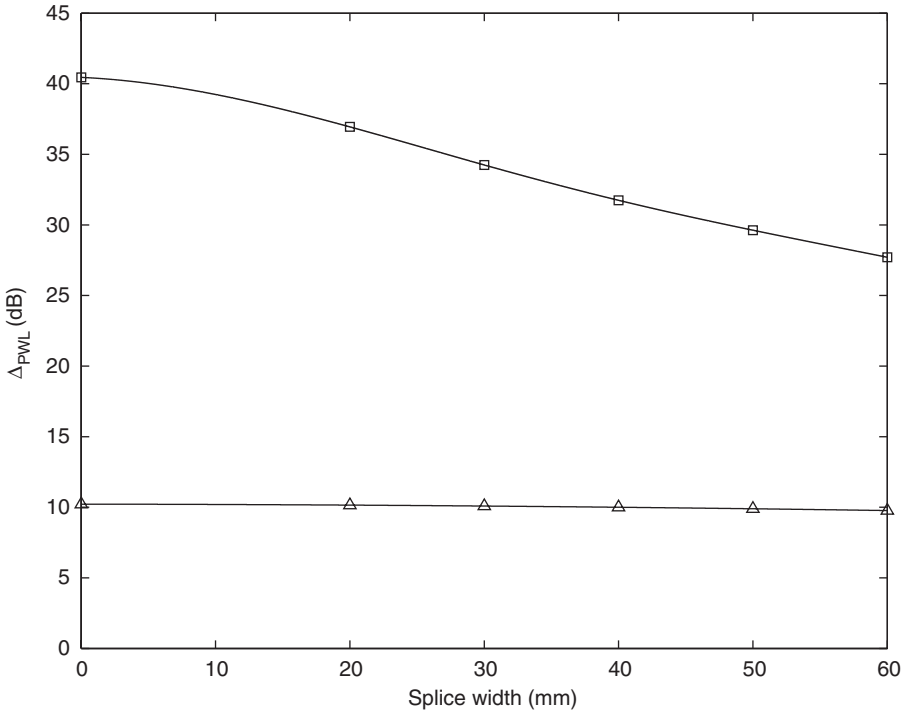

Fig. 11. Model-scale results. Variation in sound power transmission loss with splice width. Key: □, cut-back; △, sideline.

Table 3
Model-scale results. Variation in sound power transmission loss with splice width—cut-back and sideline fan speeds

Cut-back			Sideline		
Splice width (mm)	Δ_{PWL} (FEM) (dB)	Δ_{PWL} (mode-matching) (dB)	Splice width (mm)	Δ_{PWL} (FEM) (dB)	Δ_{PWL} (mode-matching) (dB)
0	40.5	40.1	0	10.2	10.0
20	36.9	—	20	10.2	—
30	34.2	—	30	10.1	—
40	31.7	—	40	10.0	—
50	29.6	—	50	9.9	—
60	27.7	—	60	9.8	—

6. Discussion

It is seen in Fig. 7 that the liner splices are predicted to scatter the acoustic energy into *all* the cut-on modes. The sign of m denotes whether the mode is spinning clockwise or counterclockwise. The cut-off ratios for $\pm m$ are equal, therefore the symmetry seen in the modal distributions about $m = 0$ is not surprising. However, it is seen in Figs. 8–10 that the azimuthal modal sound power levels are dependent on the fan speed and splice width.

At cut-back, the rotor-alone pressure field is near cut-off. Therefore, the rotor-alone modes ($m = B$) are well absorbed by the acoustic liner. It is seen in Fig. 8 that, at $m = B$, the sound power levels at the exit plane are almost independent of the splice width. At cut-back, Δ_{PWL} at $m = B$ is between 39.7 and 40.2 dB with a spliced liner (see Fig. 8), and 40.5 dB with a uniform liner (see Table 3). The liner splices only have a very small effect

on the attenuation of the rotor-alone modes, but they cause scattering into non-rotor-alone modes, with azimuthal mode orders $m \neq B$.

Scattered modes, with $|m| < B$, are more cut-on than the rotor-alone field, so less well absorbed by the acoustic liner. At each azimuthal mode order, the least attenuated mode will have radial order $n = 1$. In Table 4 there is comparison of the least attenuated modes at cut-back. (Details are provided at full and model scale. The comparison between full- and model-scale results is discussed in Appendix A.) At model scale, compare the cut-off ratios and axial decay rates of the scattered modes, with the rotor-alone mode, i.e. compare (0, 1) to (10, 1) with (12, 1). The attenuation of the scattered modes, apart from $|m| = 10$, is likely to be small. This is confirmed by the results shown in Fig. 8. Azimuthal mode orders $|m| = 0$ to $|8|$ have similar sound power levels. It is seen that for these azimuthal mode orders, it is the splice width, not the mode order, that is the most significant factor. The sound power levels range from about 110 dB (thick splice) to about 100 dB (thin splice).

At the exit plane, the composition of the BPF tone will be comprised of modes caused by scattering, and the original rotor-alone modes generated by the fan. In general, at low supersonic fan speeds, as the rotor-alone pressure field is near cut-off, the scattered modes will be a significant source of tonal noise. The sound power levels of the scattered modes can be reduced by having thinner splices. So at the cut-back fan speed, reducing the splice width is predicted to increase the sound power transmission loss at BPF, see Table 3.

At sideline, the rotor-alone pressure field is well cut-on. Therefore, rotor-alone modes ($m = B$) are poorly absorbed by the acoustic liner. At sideline, Δ_{PWL} at $m = B$ is 10.1 dB with a spliced liner (see Fig. 9), and 10.2 dB with a uniform liner (see Table 3). So, also at this higher fan speed, the liner splices only have a very small effect on the attenuation of the rotor-alone modes.

However, the scattered modes ($|m| < B$) also are well cut-on, and poorly absorbed by the acoustic liner. A comparison of the least attenuated modes at sideline is listed in Table 5. At the exit plane, the sound power levels of the scattered modes, predicted for each different splice width, are on average slightly higher at sideline

Table 4
Full- and model-scale results. Comparison between the least attenuated modes ($n = 1$) at full and model scale—cut-back fan speed

Full scale					Model scale				
(m, n)	$\zeta_{m,n}$	$\mathrm{Re}\{\alpha_x^+/k\}$	$\mathrm{Im}\{\alpha_x^+\}$	Δ_{LAM} (dB)	(m, n)	$\zeta_{m,n}$	$\mathrm{Re}\{\alpha_x^{+\star}/k^\star\}$	$\mathrm{Im}\{\alpha_x^{+\star}\}$	Δ_{LAM} (dB)
(24, 1)	1.10	0.7788	−5.8036	40.3	(12, 1)	1.10	0.7775	−5.8053	40.3
(20, 1)	1.31	1.0986	−2.1158	14.7	(10, 1)	1.30	1.0003	−2.8630	19.9
(16, 1)	1.61	1.3098	−0.9929	6.9	(8, 1)	1.58	1.2161	−1.3190	9.2
(12, 1)	2.09	1.4562	−0.4870	3.4	(6, 1)	2.04	1.3874	−0.6222	4.3
(8, 1)	3.01	1.5585	−0.2218	1.5	(4, 1)	2.88	1.5116	−0.2902	2.0
(4, 1)	5.46	1.6261	−0.0769	0.5	(2, 1)	5.01	1.5981	−0.1148	0.8
(0, 1)	—	1.6627	−0.0073	0.05	(0, 1)	—	1.6519	−0.0230	0.16

Table 5
Full- and model-scale results. Comparison between the least attenuated modes ($n = 1$) at full and model scale—sideline fan speed

Full scale					Model scale				
(m, n)	$\zeta_{m,n}$	$\mathrm{Re}\{\alpha_x^+/k\}$	$\mathrm{Im}\{\alpha_x^+\}$	Δ_{LAM} (dB)	(m, n)	$\zeta_{m,n}$	$\mathrm{Re}\{\alpha_x^{+\star}/k^\star\}$	$\mathrm{Im}\{\alpha_x^{+\star}\}$	Δ_{LAM} (dB)
(24, 1)	1.36	1.4417	−1.5668	10.9	(12, 1)	1.36	1.4418	−1.5667	10.9
(20, 1)	1.61	1.6200	−0.8555	5.9	(10, 1)	1.60	1.6025	−1.0716	7.4
(16, 1)	1.98	1.7516	−0.4822	3.4	(8, 1)	1.96	1.7263	−0.7148	5.0
(12, 1)	2.58	1.8499	−0.2626	1.8	(6, 1)	2.52	1.8234	−0.4454	3.1
(8, 1)	3.72	1.9217	−0.1274	0.9	(4, 1)	3.55	1.8987	−0.2462	1.7
(4, 1)	6.74	1.9704	−0.0459	0.3	(2, 1)	6.18	1.9541	−0.1076	0.7
(0, 1)	—	1.9971	−0.0044	0.03	(0, 1)	—	1.9900	−0.0228	0.16

compared with at cut-back (see Fig. 10; also compare Figs. 8 and 9). At sideline, the azimuthal modal sound power levels range from about 116 dB (thick splice) to about 105 dB (thin splice). This is because at sideline, owing to the increase in fan speed, there are more cut-on modes, and the modes' cut-off ratios are higher, compared with at cut-back.

At the exit plane, the sound power level at $m = B$ is over 20 dB higher than the corresponding levels of modes with $|m| < B$. In general, at high supersonic fan speeds, as the rotor-alone pressure field is well cut-on, the scattered modes will not be a significant source of tonal noise, because the dominant modes are the rotor-alone $m = B$ components of the BPF tone. Although the levels of the scattered modes are reduced by having thinner splices, at the sideline fan speed, this is not predicted to increase the sound power transmission loss at BPF, see Table 3.

The sound power transmission losses listed in Table 3, and plotted in Fig. 11, show that at the cut-back fan speed, the predicted transmission loss is higher with thinner splices. As the splice width is reduced from 60 to 20 mm, Δ_{PWL} varies from 27.7 to 36.9 dB, and with no splices Δ_{PWL} is about 40 dB. (The FE method is not suitable to be used to examine the limiting case as $ks \to 0$, because of the difficulties associated with mesh resolution with very thin splices. Therefore, it is not known how the scattered modes would be affected by very thin splices, i.e. $ks \ll 1$.) At the sideline fan speed, the predicted transmission loss is not higher with thinner splices. At this higher speed, Δ_{PWL} varies from 9.8 to 10.2 dB as the splice width is reduced from 60 to 20 mm, and with no splices Δ_{PWL} is also about 10 dB. The potential benefit of using thinner splices to reduce supersonic fan tone noise is only apparent at low supersonic fan speeds, not at higher supersonic fan speeds.

These findings are consistent with the measured results reported in Rademaker et al. [12]. At low supersonic fan speeds, one of the principal fan tone noise sources is caused by scattering, not the original rotor-alone modes generated by the supersonic fan. However, at higher supersonic fan speeds the principal fan tone noise source is the rotor-alone pressure field. Although there is scattering, the dominant noise source is the rotor-alone modes, because the rotor-alone pressure field is poorly attenuated by the acoustic lining.

The sound power levels of the scattered modes could also be reduced by decreasing the level of the sound incident on the liner. This could be achieved by two methods: the inclusion of a short section of uniform lining with no splices close to the fan, or by increasing the distance between the fan plane and the start of the spliced liner (length d in Fig. 1). The inclusion of a short section of lining with no splices near the fan will reduce the level of sound incident on the spliced liner, without generating additional scattering. Alternatively, by simply having a section of the duct near the fan with no lining could lead to a reduction in tone noise. This is because with no splices, scattering would be eliminated close to the fan. This is in the region where there is the highest in-duct sound pressure level, so the sound field will still be attenuated by nonlinear effects, because of the high pressures in this region. However, the benefit of increasing the length d is limited because the rate of nonlinear attenuation decreases with distance from the fan, and also a smaller area of the duct wall will be lined, which is likely to reduce the attenuation of other noise sources.

7. Conclusions

Three-dimensional finite-element (FE) simulations are difficult to perform at high frequencies because the problem size becomes prohibitively large with increasing frequency. Therefore, in this article a model-scale problem is proposed. Three-dimensional FE simulations are conducted at a reduced frequency.

The simulations of scattering and transmission in an acoustically lined turbofan inlet duct appear to show realistic results for a spliced liner. The numerical results show the same trends as the measurements reported in Ref. [12]: that the relative importance of the liner scattered modes is dependent on the fan speed.

At supersonic fan speeds, the rotor-alone pressure field's cut-off ratio $\zeta > 1$. At cut-back, the rotor-alone field is near cut-off: scattered modes are predicted to be a principal fan tone noise source. The level of the scattered modes can be significantly reduced by having thinner splices. However, at sideline, the rotor-alone field is well cut-on. At this fan speed, the rotor-alone modes are predicted to remain the principal fan tone noise source. The level of the scattered modes at sideline can be reduced with thinner splices. However, at high fan speeds, thinner splices are not predicted to lead to an increase in the overall sound power transmission loss. This is because the rotor-alone pressure field is well cut-on, and poorly absorbed by the duct liner.

At high fan speeds, more novel noise control methods are required to significantly improve the attenuation. A novel axially segmented liner, which is predicted to improve the attenuation of fan tones at high supersonic fan speeds, will be examined in a subsequent article on acoustic scattering at supersonic fan speeds.

Acknowledgements

We warmly acknowledge the following people with whom we have discussed the technical content of this work during the preparation of this article: R.J. Astley, M.J. Fisher, B.J. Tester (ISVR); A.J. Kempton and N.J. Baker (Rolls-Royce); H. Batard and S. Thezelais (Airbus France).

Part of this work was funded by the European fifth framework "Technology Platform" SILENCE(R).

We wish to acknowledge the continuing financial support provided by Rolls-Royce plc.

Appendix A. Comparison of results at full and model scale

The key difference between the full- and model-scale problems is that the Helmholtz number is not preserved. The aim, using a reduced frequency model-scale problem, is *not* to replicate the in-duct acoustic pressure field that would be calculated at full scale. Clearly, the number of cut-on modes and the mode shapes are different at model and full scale, so there is no expectation that the acoustic pressure will be the same in the two problems. Instead, the aim is to mimic one aspect of the acoustic transmission using the model-scale problem; namely, to predict the sound power levels, at each azimuthal mode order, and how these levels vary with different splice widths. It follows that the realistic prediction of the azimuthal modal sound power levels, also should ensure that a realistic value of the sound power transmission loss is predicted.

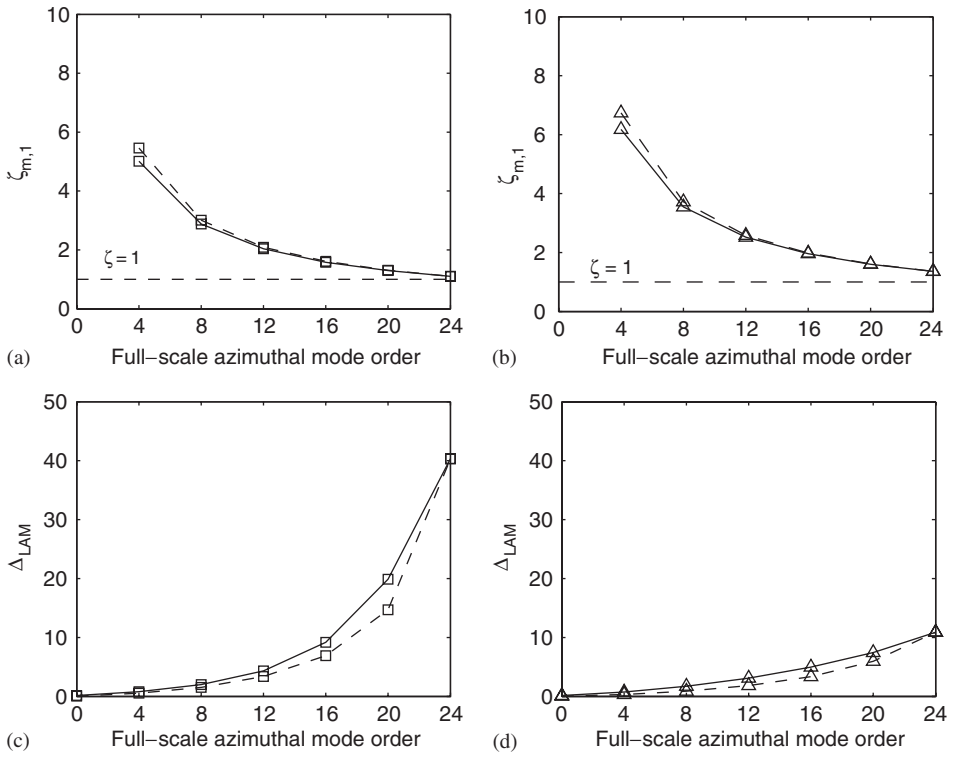

Fig. 12. Full- and model-scale results. Comparison between the least attenuated modes ($n = 1$) at full and model scale. The values of $\zeta_{m,1}$ and Δ_{LAM} are also listed in Tables 4 and 5. Key: dashed line, full scale; solid line, half-scale; □, cut-back; △, sideline.

In Section 4, the choice of $Z^\star$ is determined by matching the rotor-alone mode $(B, 1)$ at full and model scale. The other relevant modes are at azimuthal mode orders $m = B - N_s$, $B - 2N_s$, etc. It would be more difficult to find a value of $Z^\star$ that accurately matched a prescribed set of modes. Although, mode $(B, 1)$ is matched at full and model scale, how do the scattered modes compare?

It is assumed that, at each azimuthal mode order, the sound power level is mainly dependent on the least attenuated mode, which is radial mode order $n = 1$. In Tables 4 and 5 the least attenuated modes, at full and model scale, are compared at the cut-back and sideline fan speeds, respectively. The sound power levels will depend on how well the scattered modes are absorbed by the acoustic liner. At each azimuthal mode order, the cut-off ratio $\zeta_{m,1}$ and transmission loss Δ_{LAM}, of the least attenuated modes, at full and model scale and at both fan speeds, are shown plotted in Fig. 12. There is a close correlation between the full- and model-scale values of $\zeta_{m,1}$, and similarly between the values of Δ_{LAM}.

As well as the close agreement between the full- and model-scale values of $\zeta_{m,1}$ and Δ_{LAM}; also, at low azimuthal mode orders, the values of Δ_{LAM} are small because of the high values of the cut-off ratio. These are the two crucial factors which suggest that it is possible to calculate, at a reduced frequency, realistic azimuthal modal sound power levels. From the work of Rice, e.g. see Refs. [19–21], it is well known that sound attenuation in a lined duct is dependent on the modes' cut-off ratios, in addition to the wall impedance Z. In a lined duct, well cut-on modes tend to be poorly absorbed, regardless of the value of Z. This is illustrated in Figs. 13 (full scale) and 14 (model scale), which show how Δ_{LAM} varies with Z, for different azimuthal mode orders, at the cut-back fan speed.

Compare the contour plots at full and model scale, i.e. $m = 24$ and 12; $m = 16$ and 8; $m = 8$ and 4; and $m = 0$. The shape of the contours are similar, but not the same at full and model scale. However, the contour levels are comparable at full and model scale. Also, note that *all* these levels are relatively low, compared with the values at $m = 24$ or 12. The values of Z and $Z^\star$, at the cut-back fan speed, are shown in Figs. 13 and 14. The choice of $Z^\star$ will determine the axial decay rates of the rotor-alone and the scattered modes. The low-order azimuthal modes have high cut-off ratios, so the predicted values of Δ_{LAM} are small, over a wide range

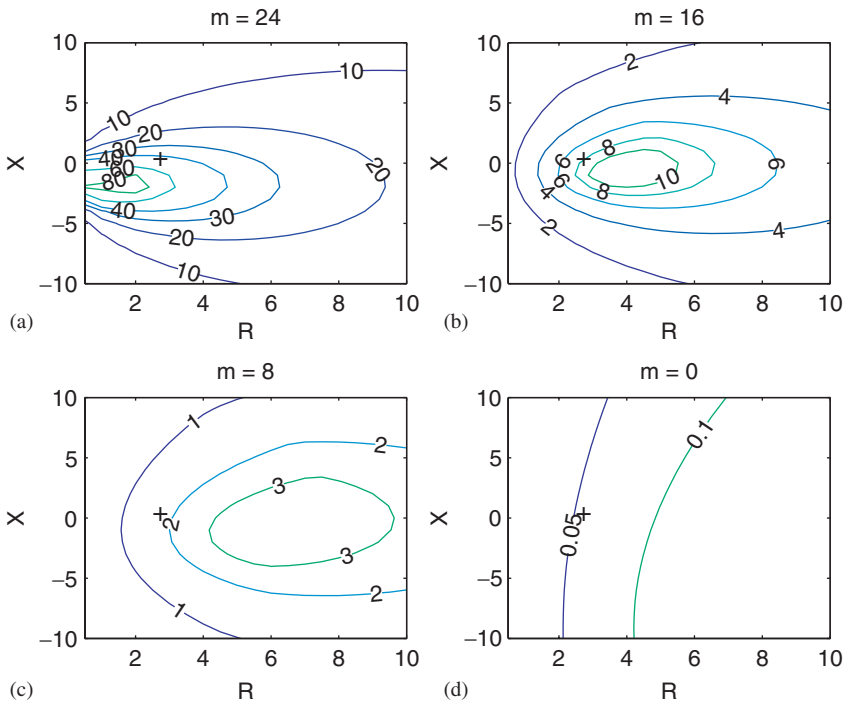

Fig. 13. Full-scale results. Contour plot of Δ_{LAM} in (R, X)-plane—cut-back fan speed. Full-scale impedance $Z = 2.50 + 0.57\,\mathrm{i}$ (+). Azimuthal mode orders (a) $m = 24$ to (d) $m = 0$.

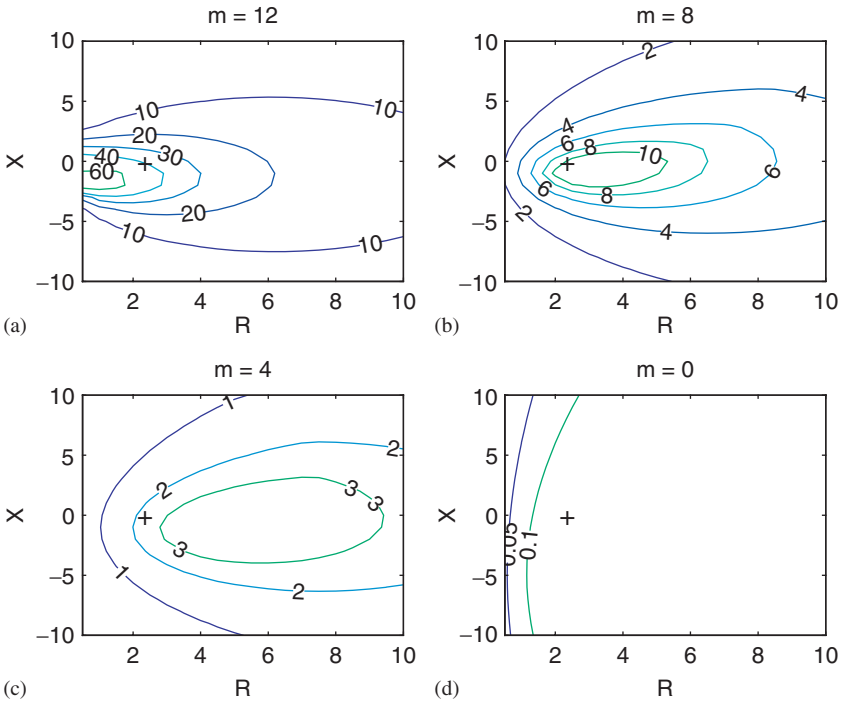

Fig. 14. Model-scale results. Contour plot of Δ_{LAM} in (R, X)-plane—cut-back fan speed. Model-scale impedance $Z^{\star} = 2.12 + 0.01\,\mathrm{i}$ (+). Azimuthal mode orders (a) $m = 12$ to (d) $m = 0$.

of possible values of the impedance. Therefore, the choice of $Z^{\star}$ is less significant for the scattered modes, compared with the rotor-alone mode, whence it is crucial that the correct axial decay rate is utilized at model scale.

In order to provide additional evidence of the suitability of using this model-scale problem, it is necessary to calculate a benchmark example at full scale, to permit a direct comparison between results at full and model scale. In this example a FE simulation at full scale has been performed, but only at cut-back ($kb = 26.6$). The example is based on the full- and model-scale problems already defined. However, to enable the FE simulations to be run on a high-performance PC, the length of the inlet duct is halved in order to reduce the problem size. (Otherwise at $kb = 26.6$ the problem could not be run on the PC because there was not sufficient memory.) Hence for this benchmark test case $L = 0.55\,\mathrm{m}$ and $l = 0.4\,\mathrm{m}$, instead of the actual values listed in Table 1.

Fig. 15 shows a comparison of the azimuthal modal sound power levels at full and model scale, with different splice widths from $s = 20$ to 60 mm. Note that all the results have been corrected so that, at the fan plane, the sound power level of mode $(B, 1)$ is the same at model and full scale. It is seen that at the exit plane the predicted values of the sound power level at full and model scale are in close agreement. The best agreement is at full-scale azimuthal mode orders $m = 24$ (i.e. $m = B$) and $m = 0$. The close agreement at $m = B$ indicates that the change in impedance used at full and model scale, i.e. $Z \to Z^{\star}$, has led to a realistic attenuation of azimuthal mode $m = B$ being calculated at model scale.

In general, the predicted sound power levels of the non-rotor-alone azimuthal mode orders ($m \neq B$) are a little higher at full scale than at model scale. This is not surprising because one of the key differences, between the full- and model-scale problem, is that at model scale there are fewer cut-on modes. Therefore, energy is scattered into less modes at model scale. Although there are small differences between the absolute levels of the two sets of results, both the full- and model-scale results show the same variation with changes in splice width.

In Table 6, a comparison of the predicted sound power transmission losses at full and model scale, with different splice widths, is listed. The predicted values of Δ_{PWL} at full and model scale are in close agreement.

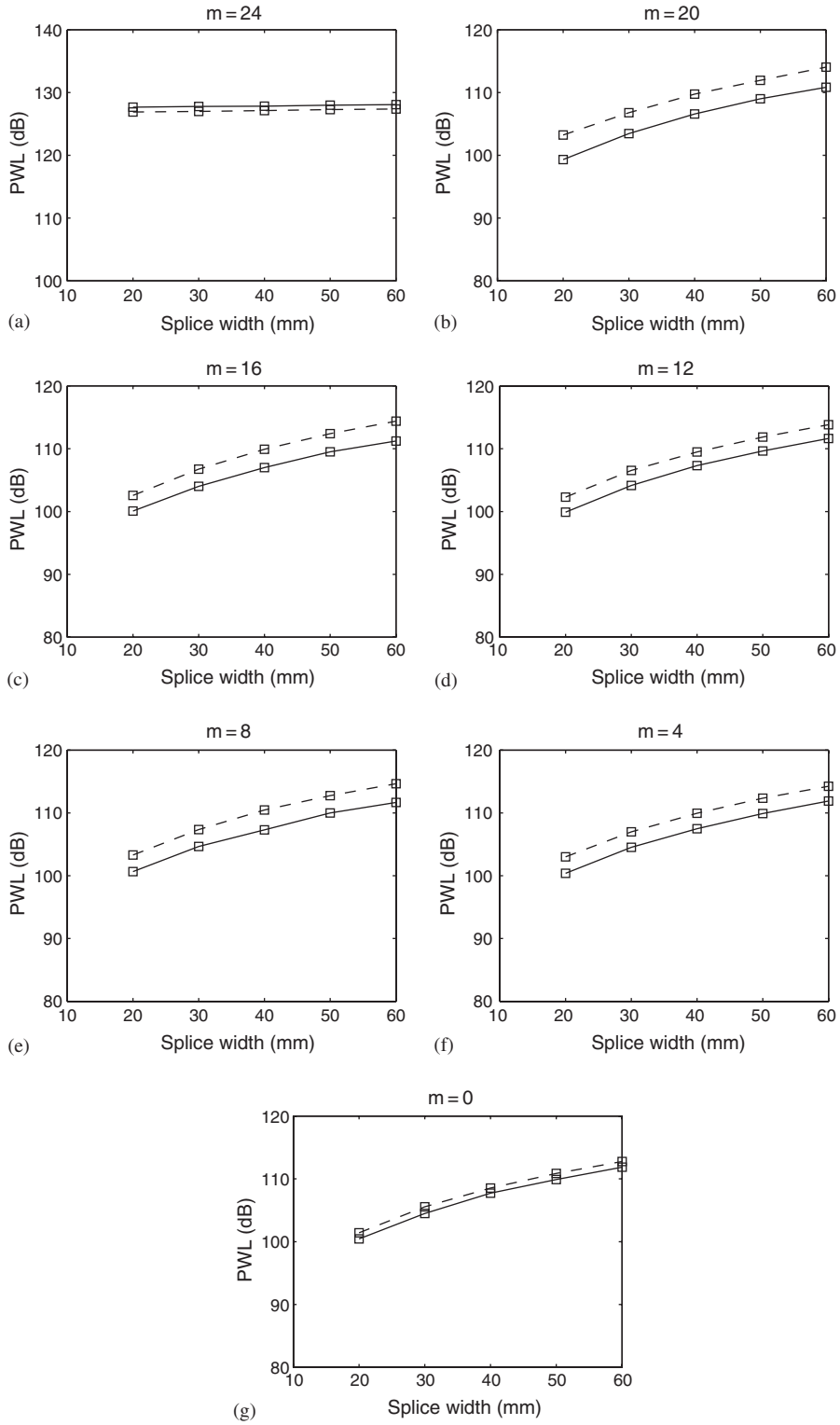

Fig. 15. Benchmark example. Variation in sound power levels at the exit plane with different splice widths. Full-scale azimuthal mode orders (a) $m = 24$ to (g) $m = 0$. Key: dashed line, full scale; solid line, half-scale.

Table 6
Benchmark example. Variation in sound power transmission loss with splice width

Splice width (mm)	Δ_{PWL} (dB)	
	Full scale	Model scale
20	20.7	20.0
30	20.4	19.8
40	19.9	19.6
50	19.3	19.2
60	18.7	18.8

Finally, it is interesting to compare, at the cut-back fan speed, the model-scale results shown in Fig. 10 with the benchmark example shown in Fig. 15. In the benchmark example, the duct length L and liner length l that is used, are only half their actual lengths. However, it can be seen that the sound power levels of azimuthal mode orders $m = 16, 12, 8, 4$ and 0 are quite similar in both sets of results, even though two different liner lengths are used. The length of the acoustic liner seems to have little affect on these modes, because they are well cut-on. Therefore, unless these scattered modes can be absorbed, the sound power transmission loss will be limited by these poorly attenuated modes; increasing the length of the liner may not lead to a significant increase in Δ_{PWL}. However, at this low supersonic fan speed, reducing the splice width will increase Δ_{PWL} because this will reduce the sound power levels of the non-rotor-alone scattered modes.

References

[1] J.M. Tyler, T.G. Sofrin, Axial flow compressor noise studies, *SAE Transactions* 70 (1962) 309–332.
[2] D.L. Lansing, W.E. Zorumski, Effects of wall admittance changes on duct transmission and radiation of sound, *Journal of Sound and Vibration* 27 (1) (1973) 85–100.
[3] J.F. Unruh, Finite length tuning for low-frequency lining design, *Journal of Sound and Vibration* 45 (1) (1976) 5–14.
[4] W. Watson, Noise suppression characteristics of peripherally segmented duct liners, NASA TP-1904, 1981.
[5] C.R. Fuller, Propagation and radiation of sound from flanged circular ducts with circumferentially varying wall admittances, I: semi-infinite ducts, *Journal of Sound and Vibration* 93 (3) (1984) 321–340.
[6] C.R. Fuller, Propagation and radiation of sound from flanged circular ducts with circumferentially varying wall admittances, II: finite ducts with sources, *Journal of Sound and Vibration* 93 (3) (1984) 341–351.
[7] T. Elnady, H. Bodén, R. Glav, Application of the point matching method to model circumferentially segmented non-locally reacting liners, AIAA 2001-2202, 2001.
[8] T. Elnady, H. Bodén, Hard strips in lined ducts, AIAA 2002-2444, 2002.
[9] M.C.M. Wright, Hybrid analytical/numerical method for mode scattering in azimuthally non-uniform duct liners, *Journal of Sound and Vibration*, 2005, in press.
[10] W. Watson, A finite element simulation of sound attenuation in a finite duct with a peripherally variable liner, NASA TM-74080, 1977.
[11] R.J. Astley, N.J. Walkington, W. Eversman, Transmission in flow ducts with peripherally varying liners, AIAA 80-1015, 1980.
[12] E.R. Rademaker, P. Sijtsma, B.J. Tester, Mode detection with an optimised array in a model turbofan engine intake at varying shaft speeds, AIAA 2001-2181, 2001.
[13] A. McAlpine, M.C.M. Wright, H. Batard, S. Thezelais, Finite/boundary element assessment of a turbofan spliced intake liner at supersonic fan operating conditions, AIAA 2003-3305, 2003.
[14] W. Eversman, Theoretical models for duct acoustic propagation and radiation, in: H.H. Hubbard (Ed.), Aeroacoustics of Flight Vehicles: Theory and Practice, Vol. 2: Noise Control, NASA RP-1258, 1991, pp. 101–163.
[15] C.L. Morfey, Sound transmission and generation in ducts with flow, *Journal of Sound and Vibration* 14 (1971) 37–55.
[16] M.K. Myers, On the acoustic boundary condition in the presence of flow, *Journal of Sound and Vibration* 71 (3) (1980) 429–434.
[17] ACTRAN/AE User manual, Free Field Technologies, 16 Place de l'Université, B-1348, Louvain-la-Neuve, Belgium. http://www.fft.be/.
[18] B. Regan, J. Eaton, Modelling the influence of acoustic liner non-uniformities on duct modes, *Journal of Sound and Vibration* 219 (5) (1999) 859–879.

[19] E.J. Rice, Acoustic liner optimum impedance for spinning modes with mode cutoff ratio as the design criterion, AIAA 76-516, 1976 .
[20] E.J. Rice, Inlet noise suppressor design method based upon the distribution of acoustic power with mode cutoff ratio, *Advances in Engineering Science*, Vol. 3, NASA CP-2001, 1976, pp. 883–893.
[21] E.J. Rice, Optimum wall impedance for spinning modes—a correlation with mode cutoff ratio, *Journal of Aircraft* 16 (5) (1979) 336–343.